EARTH'S CRYOSPHERE
SCIENTIFIC JOURNAL

Kriosfera Zemli, 2017, vol. XXI, No. 1, pp. 60–66 **http://www.izdatgeo.ru**

RELIABILITY OF BASEMENTS AND STRUCTURES IN CRYOLITHOZONE

DOI: 10.21782/EC2541-9994-2017-1(60-66)

INFLUENCE OF VERTICAL SEASONAL COOLING DEVICES ON SOIL HEAT AND MOISTURE TRANSFER

P.P. Permyakov[1,2], S.P. Varlamov[2], M.N. Zhelezniak[2]

[1] *Larionov Institute of the Physical-Technical Problems of the North, SB RAS, 1, Oktyabrskaya str., Yakutsk, 677891, Russia; permyakov2005@mail.ru*
[2] *Melnikov Permafrost Institute, SB RAS, 36, Merzlotnaya str., Yakutsk, 677010, Russia; fe@mpi.ysn.ru*

A model is suggested for simulation of soil heat and moisture transfer around a single seasonal cooling device (a thermosyphon). The numerical results are compared with temperature measurements in the field. The revealed heat and moisture patterns around a thermosyphon show seasonal dynamics.

Model of heat and moisture transfer, foundations of structures, thermosyphon, prediction

INTRODUCTION

Global change for the past three decades poses problems to construction and operation of buildings and utilities on permafrost. Warming induces degradation of permafrost, uneven heaving, soil subsidence and creep, which in its turn causes deformation of basements and foundations and settlement of structures. Therefore, special engineering solutions are required for maintaining the stability of structures, including the worldwide use of thermosyphons [*Chen et al., 2000; Dolgikh et al., 2011b; Velchev et al., 2013*]. Seasonal cooling devices (thermosyphons) can accumulate and store cold and change the patterns of soil heat and moisture transport. This paper presents a numerical model of heat and moisture transfer around a thermosyphon.

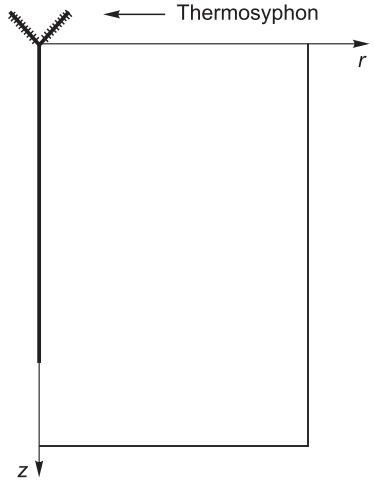

Fig. 1. Modeling domain: zone around a thermosyphon.

PROBLEM FORMULATION

Heat and moisture transfer around a thermosyphon (Fig. 1) can be described by the system of differential equations in cylindrical coordinates [*Permyakov and Ammosov, 2003; Dolgikh et al., 2011a; Anikin et al., 2013*]

$$c\frac{\partial T}{\partial \tau}=\frac{1}{r^{\nu}}\frac{\partial}{\partial r}\left(r^{\nu}\lambda\frac{\partial T}{\partial r}\right)+\frac{\partial}{\partial z}\left(\lambda\frac{\partial T}{\partial z}\right)- c_{\mathrm{w}}V_r\frac{\partial T}{\partial r}-c_{\mathrm{w}}V_z\frac{\partial T}{\partial z}+L\frac{\partial W_{\mathrm{ice}}}{\partial \tau}; \quad (1)$$

$$\frac{\partial \theta_{\mathrm{w}}}{\partial \tau}=\frac{1}{r^{\nu}}\frac{\partial}{\partial r}\left(r^{\nu}k_{\mathrm{f}}\frac{\partial H}{\partial r}\right)+\frac{\partial}{\partial z}\left(k_{\mathrm{f}}\frac{\partial H}{\partial z}\right)-\frac{\partial \theta_{\mathrm{ice}}}{\partial \tau}; \quad (2)$$

$$\frac{\partial W_{\mathrm{w}}}{\partial \tau}=\frac{1}{r^{\nu}}\frac{\partial}{\partial r}\left(r^{\nu}k\frac{\partial W_{\mathrm{w}}}{\partial r}\right)+\frac{\partial}{\partial z}\left(k\frac{\partial W_{\mathrm{w}}}{\partial z}\right)-\frac{\partial W_{\mathrm{ice}}}{\partial \tau}, \quad (3)$$

$$(r,z)\in\Omega,\ \ \tau>0,\ \ \Omega=[0,R]\times[0,H_1].$$

The system of equations includes three unknowns and is solved with an additional function for the amount of unfrozen water

$$W_{\mathrm{w}}=W_{\mathrm{ufw}}(T,W). \quad (4)$$

The boundary condition of heat exchange on the evaporator wall, present in winter and absent in summer, is

$$r\lambda\frac{\partial T}{\partial n}=\begin{cases}r\alpha_{\mathrm{eff}}\left(T_{\mathrm{ev}}-T\right)T_{\mathrm{air}}<0,\\ 0,\qquad T_{\mathrm{air}}\geq 0,\end{cases}\quad \text{at } r=r_0,$$

where T is the temperature, K; c, c_w are the heat capacity of soil and water, respectively, J/(m^3·K); τ is the time, s; ρ is the density of soil skeleton, kg/m^3; $W = W_{ice} + W_w$ is the total weight soil moisture content, at the account of ice (W_{ice}) and unfrozen water (W_w); λ is the soil thermal conductivity, W/(m·K); r, z are the spatial coordinates (r is the radius around the thermosyphon axis and z is the distance along the vertical axis (depth), m); L is the specific heat of phase change, J/m^3; $V = (V_r, V_z)$ is the infiltration rate, m/s; k is the diffusion coefficient, m^2/s; H is the head pressure, Pa; $H = P - z\rho_w g$; P is the suction pressure, Pa; ρ_w is the water density, kg/m^3; g is the acceleration due to gravity, m/s^2; k_f is the filtration coefficient, m/s; $\theta = \theta_{ice} + \theta_w$ is the total volumetric moisture content, at the account of ice (θ_{ice}) and unfrozen water (θ_w); α_{eff} is the effective heat transport to the thermosyphon outer surface, W/(m^2·K); $\nu = 0, 1$ ($\nu = 0$ in Cartesian coordinates and $\nu = 1$ in cylindrical coordinates); R and H_1 are, respectively, the width and depth of the modeling domain Ω, m; $\frac{\partial T}{\partial n}$ is the derivative along the normal n; T_{ev} and T_{air} are the temperatures of the evaporator and the ambience (air), K.

Equation (1) describes soil freezing and thawing with regard to heat transport by moisture. Moisture transport and ice segregation are given by equations (2)–(4). Both equations (2) and (3) are applicable to predict the moisture regime; Richard's equation (2) is commonly used in both saturated and unsaturated soils while (3) is rather for unsaturated soils.

SOLUTION ALGORITHM

The system of equations (1)–(3) is nonlinear and the simulation is implemented as an implicit difference scheme with iterations [*Permyakov and Ammosov, 2003*]. The system is split into a chain of 1D linear solutions:

$$\begin{cases} c^s_{\text{eff}} \dfrac{\tilde{T}_i^{s+1} - \breve{T}_i}{\tau} = a\left(r^\nu \lambda^s \tilde{T}^{s+1}_{\bar{r}}\right)_{\hat{r}} - C_1 \tilde{T}^{s+1} + Li\left(T^s\right) W^s_{\bar{\tau}}, \\ \mu^s \dfrac{\tilde{P}_i^{s+1} - P_i^s}{\tau} + \dfrac{\theta_i^s - \breve{\theta}_i}{\tau} = a\left(r^\nu k_f^s \eta^s \tilde{P}^{s+1}_{\bar{r}}\right)_{\hat{r}}, \\ \dfrac{\tilde{W}_i^{s+1} - \breve{W}_i}{\tau} = a\left(k^s \eta^s \tilde{W}^{s+1}_{\bar{r}}\right)_{\hat{r}}, \end{cases} \quad (5)$$

$$\begin{cases} c^s_{\text{eff}} \dfrac{T_j^{s+1} - \tilde{T}_j^{s+1}}{\tau} = \left(\lambda^s T^{s+1}_{\bar{z}}\right)_{\hat{z}} - C_2 T^{s+1} + Li\left(\tilde{T}^{s+1}\right) \tilde{W}^{s+1}_{\bar{\tau}}, \\ \mu^s \dfrac{P_j^{s+1} - \tilde{P}_j^{s+1}}{\tau} + \dfrac{\tilde{\theta}_j^{s+1} - \breve{\theta}_j}{\tau} = \left(k_f^s \eta^s P^{s+1}_{\bar{z}}\right)_{\bar{z}} - \left(k_f^s\right)_{\hat{z}}, \\ \dfrac{W_j^{s+1} - \tilde{W}_j^{s+1}}{\tau} = \left(k^s \eta^s W^{s+1}_{\bar{z}}\right)_{\hat{z}}, \end{cases} \quad (6)$$

where $a = \dfrac{\nu + 1}{r^{\nu+1}_{i+1/2} - r^{\nu+1}_{i-1/2}}$, $\eta = 1 - i(T)$, $i(T) = W_{ice}/W$,

$$c_{\text{eff}} = c + L \frac{\partial W_{ufw}(T, W)}{\partial T},$$

$$C_1 \tilde{T}^{s+1} = c_w \left(V^-_{\nu, i+1/2} \tilde{T}^{s+1}_r + V^+_{\nu, i-1/2} \tilde{T}^{s+1}_{\bar{r}}\right),$$

$$C_2 T^{s+1} = c_w \left(V^-_{z, j+1/2} T^{s+1}_z + V^+_{z, j-1/2} T^{s+1}_{\bar{z}}\right),$$

$$\left(\lambda^s T^{s+1}_{\bar{z}}\right)_{\hat{z}} = \frac{2}{h_j + h_{j+1}} \left(\lambda^s_{j+1/2} \frac{T^{s+1}_{j+1} - T^{s+1}_j}{h^+_j} - \lambda^s_{j-1/2} \frac{T^{s+1}_j - T^{s+1}_{j-1}}{h^-_j}\right),$$

h_{j+1} and h_j refer to the grid spacing; T_j, P_j, W_j, θ_j are grid functions of temperature, pressure, weight and volumetric moisture; $\mu^s = \partial \theta^s_w / \partial P$ is the volumetric moisture as a function of capillary pressure; η, i are dimensionless coefficients (of the shares of ice and water, respectively, found from $W = W_{ice} + W_w$, where $i = W_{ice}/W$, $\eta = 1 - i$); the superscript s is the iteration number.

The input data for the numerical experiment correspond to the climate conditions of Yakutsk city. The third-order boundary condition is specified on the surface of the domain Ω at $z = 0$ as

$$\lambda \frac{\partial T}{\partial z} = \alpha \left(T - T_{air}\right)$$

for thermal conductivity; the effective heat loss α includes the insulation effect of vegetation and snow. The amounts of atmospheric precipitation and evaporation from the ground surface are included in equations (2) and (3). The values of mean monthly air temperature T_{air}, the effective heat loss α, and the amounts of precipitated and evaporated moisture are

Table 1. **Boundary condition parameters on ground surface**

Parameter	Month											
	I	II	III	IV	V	VI	VII	VIII	IX	X	XI	XII
Air temperature T_{air}, K	231.5	238.4	251.1	265.4	278.1	287.3	290.8	287.1	278.7	265.0	245.9	234.7
Effective heat loss α, W/(m^2·K)	0.65	0.56	0.56	0.80	13.6	20.3	20.8	19.8	13.8	3.87	1.67	0.85
Precipitated moisture, mm	5.5	4.5	3.0	5.5	9.0	16.5	21.5	21.0	23.0	10.0	8.0	6.0
Evaporated moisture, mm	0.2	0.15	1.0	5.0	22.75	34.5	35.0	24.0	5.5	1.0	0.2	0.2

listed in Table 1. The boundary conditions on the sides and base of the domain Ω correspond to zero heat and moisture transport.

The soil lithology changes with depth as: top soil (0–0.3 m); pale yellow clay silt (0.3–0.6 m); fine sand (0.6–8.4 m); and fine sand with quartz pebble below 8.4 m. The modeling includes unsaturated and non-saline soils at construction sites in Yakutsk city, with their total moisture distributed unevenly taking into account annual water budget. Thermophysical and mass exchange parameters are specified according to data of the temperature monitoring station of Yakutsk [*Pavlov, 1979*]. Temperature, total moisture, and ice content dependences of these parameters for different soil types were reported earlier [*Permyakov and Ammosov, 2003*]. The effective heat transport to the evaporator outer surface (heat loss) α_{eff} is assumed to be 2.8 W/(m^2·K) according to technical specifications of the thermosyphon and field measurements.

NUMERICAL RESULTS

Experiment 1

Ground temperature curves for the site of *Triumf* stadium in Yakutsk were obtained by logging at a thermosyphon [*Bolshev et al., 2014*] and numerically (Fig. 2). The thermosyphon with an outer diameter of 77 mm was filled with cooling agent-22 and installed to a depth of 10 m. In October 2010 (beginning of the experiment), drilling stripped unfrozen soil (active layer) at a depth of 3.5–8.3 m. In the course of its operation, the thermosyphon cooled down the soil (Fig. 2) and produced a block of ice-rich ground growing at a rate equal to the cooling rate. As the thermosyphon ran, frozen ground froze up further and the ice-rich zone expanded. After summer warming, some amount of soil around the thermosyphon remained frozen (Fig. 2) and maintained a cold (–3 °C) temperature of the foundation soil. The field and computed temperature curves agree quite well (Fig. 2).

Late March temperature, total moisture, and ice content variations with depth around the thermosyphon were estimated for three years (Fig. 3, I–III) relative to the initial patterns of temperature and moisture based, respectively, on logging in a monitoring borehole (on 21.10.2010) and on engineering surveys. The thermosyphon operated in winter since the air temperature became negative. Simulations show the ground to cool down from October to March while moisture migrates toward the zone of cooling and produces an ice cover growing in size from year to year.

Experiment 2

Thermosyphons have been successfully used to stabilize soils under different engineering structures [*Dolgikh et al., 2011a*]. Experiment 2 focused on temperature and moisture patterns to a depth of 30 m within a distance of D_0 = 0.04 m around a thermosyphon. The calculations were performed relative to the initial temperature distribution and total soil moisture as shown in Fig. 4, I. Unfrozen soil with a total moisture of 15 % occurred at depths between 10 and 20 m. The temperature, soil moisture, and ice content patterns a year after the installation of the thermosyphon in the end of April were as follows (Fig. 4, II). In

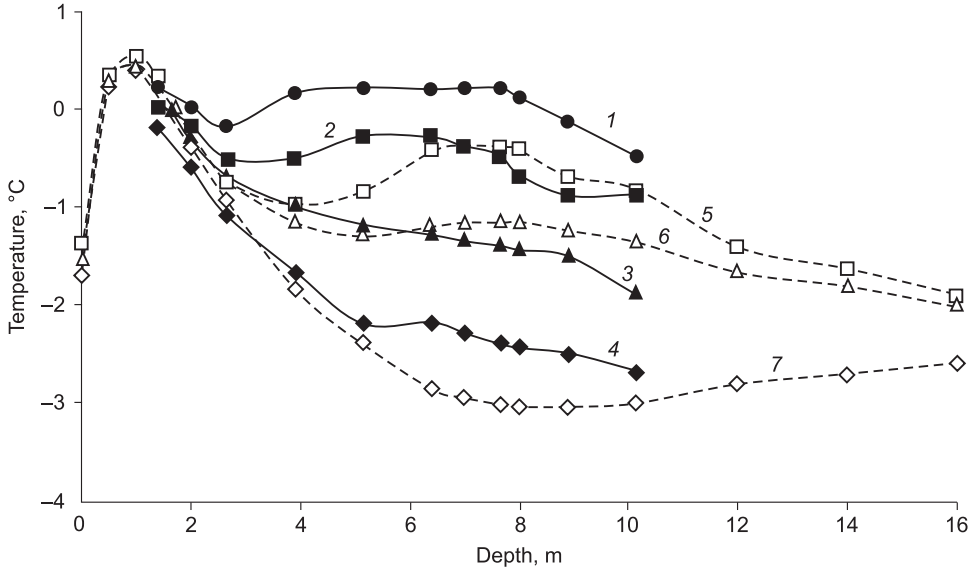

Fig. 2. Ground temperature patterns at depths of field measurements at the *Triumf* site. Measured and computed data, compared.

Curve numbers correspond to field measurements on 21.10.2010 (*1*, initial value), 17.10.2011 (*2*), 21.10.2012 (*3*), 21.10.2013 (*4*) and to simulation results for 21.10.2011 (*5*), 21.10.2012 (*6*), 21.10.2013 (*7*).

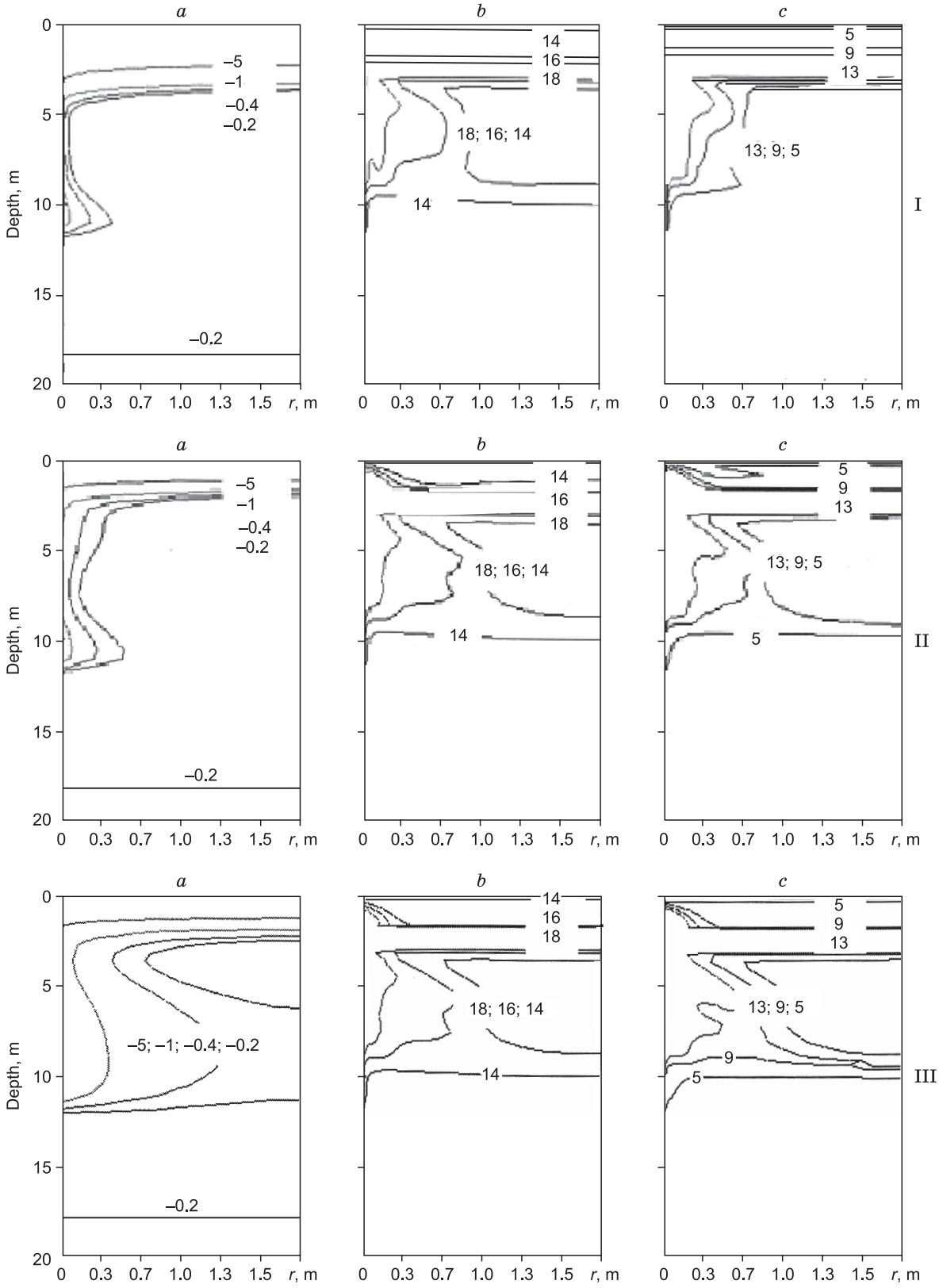

Fig. 3. Variations of ground temperature, °C (*a*), total moisture, % (*b*), and ice content, % (*c*) off the thermosyphon axis, for different times:

March 2011, first year (I); March 2012, second year (II); March 2013, in 3 years (III).

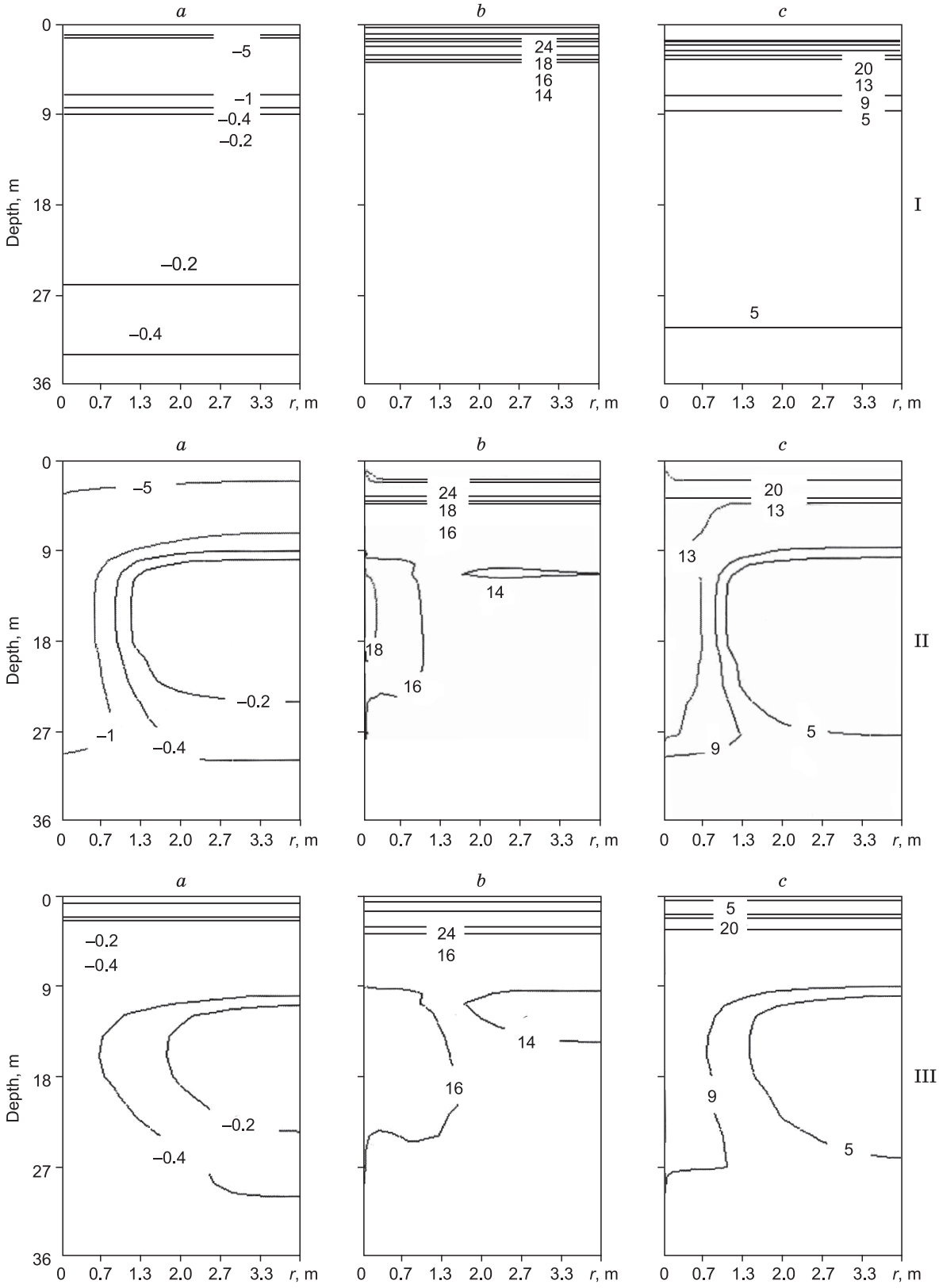

Fig. 4. Initial patterns of temperature, °C (*a*), total moisture, % (*b*), and ice content, % (*c*) off the thermosyphon axis, for different times:

Late October (I), March, first year (II), October, first year (III), March, in 2 years (IV), March, in 3 years (V).

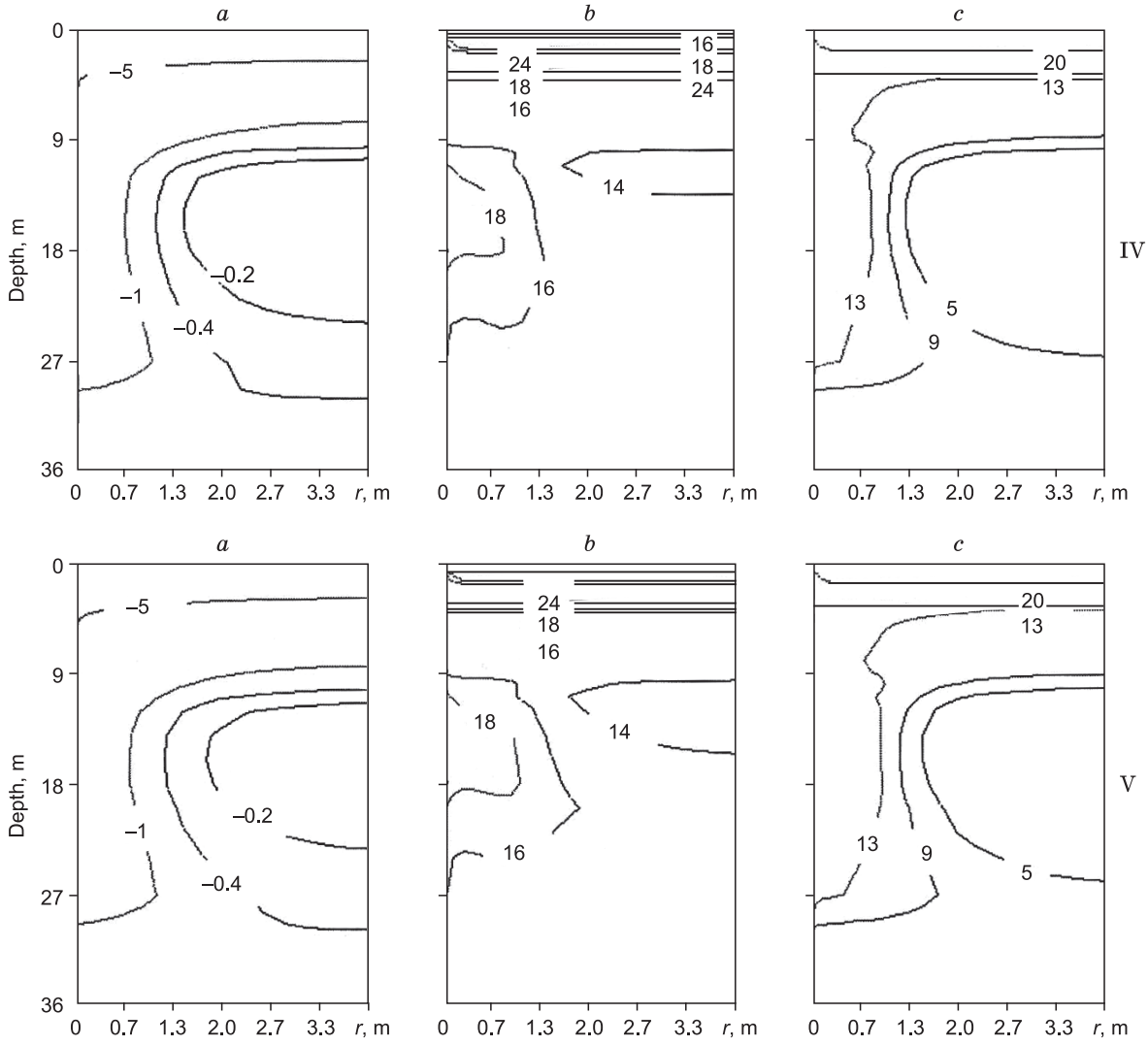

Fig. 4 (continued).

winter, the circulation of coolants induced migration of pore water and produced a 1 m thick layer of ice-rich soil (Fig. 4, II, *c*), with its thickness reducing in the end of the summer season (Fig. 4, III).

The thermosyphon began operating at the onset of the winter season; it cooled down the adjacent ground and caused accumulation of moisture around the evaporator by the segregation mechanism. The radius of the frozen layer increased successively relative to that in the previous years. The process repeated periodically every year: negative temperature set up, decreased further, and an ice cover formed and grew thus maintaining the cold temperature of permafrost by consuming much heat for phase change (Fig. 4, IV–V).

CONCLUSIONS

The suggested algorithm (5), (6), which takes into account moisture transport during soil freezing, allows simulating and predicting the temperature and moisture patterns around a vertical thermosyphon. The simulation results have been checked against field measurements at the site of *Triumf* stadium in Yakutsk city, and the computed and measured data showed good agreement.

The numerical experiments allowed estimating the growth of the ice-rich layer as a result of moisture migration around the evaporator during the thermosyphon operation. Thermophysical calculations and temperature predictions should be made with due regard for this process. Thus, the use of themosyphons for freezing soil under buildings and utilities on permafrost can ensure their stability in the conditions of changing climate.

References

Anikin, G.V., Plotnikov, S.N., Spasennikova, K.A., 2013. Calculation of soil freezing rate under the influence of a solitary thermosyphon. Kriosfera Zemli XVII (1), 51–55.

Bolshev, K.N., Ivanov, V.A., Lebedev, M.P., Stepanov, A.A., Timofeev, A.M., 2014. The results of the temperature field monitoring at foundation of "Triumph" stadium in Yakutsk. J. Eng. Heilongjiang Univ. V (3), 266–269.

Chen, R.J., Cheng, G.D., Li, S.X., 2000. Development and prospect of research on application of artificial ground freezing. Chinese J. Geotechnical Eng. 22, 40–44.

Dolgikh, G.M., Okunev, S.N., Anikin, G.V., Maramygina, M.S., Dolgikh, S.N., 2011a. Heat and mass transfer in vertical tubes of ammonia-based thermosyphons, in: Problems of Permafrost Engineering Science. Proc. IX Intern. Symp. (3–7 September 2011, Mirnyi). Institute of Permafrost, Yakutsk, pp. 285–287. (in Russian)

Dolgikh, G.M., Okunev, S.N., Zaharova, V.N., Strizhkov, S.N., Vlasov, V.F., 2011b. Permafrost confinement of moisture migration under the Vilyui Hydro-3 dam stabilized by thermosyphons: Predictive modeling, in: Problems of Permafrost Engineering Science. Proc. IX Intern. Symp. (3–7 September 2011, Mirnyi). Institute of Permafrost, Yakutsk, pp. 281–283. (in Russian)

Pavlov, A.V., 1979. Landscape Thermophysics. Nauka, Novosibirsk, 286 pp. (in Russian)

Permyakov, P.P., Ammosov, A.P., 2003. Modeling of Man-caused Pollution in Permafrost. Nauka, Novosibirsk, 224 pp. (in Russian)

Velchev, S., Okunev, S., Rilo, I., 2013. Preserving the perennial for building the future. Neftegazovaya Vertikal 17, 36–39.

Received September 20, 2015